JOURNAL OF THEORETICAL
AND APPLIED MECHANICS
64, 2, pp. 115–129, Warsaw 2026
https://doi.org/10.15632/jtam-pl/220006

NONLINEAR DAMPING IDENTIFICATION USING AN EXTENDED STABILIZED LAYERS METHOD

Nourhaine YOUSFI*, Rania MAKTOUF, Ali AKROUT, Lassaad WALHA, Mohamed HADDAR

Mechanics, Modelling and Production Laboratory (LA2MP), National Engineering School of Sfax, University of Sfax, Sfax, Tunisia

*corresponding author, *nourhainegem@gmail.com*

In many practical mechanical systems, the dynamic response is strongly influenced by time-varying stiffness, often coupled with nonlinear damping effects. Neglecting stiffness variability may lead to inaccurate predictions of vibration amplitudes and energy dissipation. This study is the first to extend and apply the stabilized layers method for nonlinear (SLMnl) damping identification to mechanical systems with time-varying stiffness. The SLMnl,kv is developed for multi-degree-of-freedom systems exhibiting nonlinear damping and time-varying stiffness. The effectiveness of the proposed method is demonstrated through its application to a spur gear pair system characterized by nonlinear damping and time-varying mesh stiffness.

Keywords: nonlinear damping identification; stabilized layers method; time-varying stiffness; system identification; sidebands.

1. Introduction

Several types of damping mechanisms can be found in mechanical systems (Qu *et al.* 2024), including viscous damping, Coulomb damping, and hysteretic damping (Liu *et al.*, 2022; Clough & Penzien, 1993). Damping identification plays a crucial role in dynamic system analysis, as accurate estimation of damping parameters is essential for design and analysis (Paz, 1991). Conventional damping identification techniques often suffer from several drawbacks, such as high computational cost and strong sensitivity to measurement noise (Zahid *et al.*, 2020). Considerable efforts have therefore been dedicated to overcoming these limitations. Among them, the stabilized layers method (SLM), introduced by Lisitano *et al.* (2018), has demonstrated good robustness and reliability by providing damping coefficients with clear physical interpretation. Nevertheless, the formulation proposed by Bonisoli *et al.* (2019) remains restricted to equivalent linear representations. In real engineering applications, numerous mechanical systems exhibit nonlinear damping phenomena arising from sources such as material hysteresis, interface friction, and geometric nonlinearities. These nonlinear effects become particularly significant under large vibration amplitudes, and ignoring them may result in substantial modeling errors (Balasubramanian *et al.*, 2018; Amabili *et al.*, 2016; Haghdoust *et al.*, 2018). Consequently, current research trends increasingly focus on parametric identification strategies capable of distinguishing linear damping effects from nonlinear contributions, thereby improving the understanding and characterization of energy dissipation mechanisms. Al-hababi *et al.* (2020) provided a comprehensive review of nonlinear damping identification methods, highlighting both their strengths and fundamental limitations. Their study concluded that approaches accounting for nonlinear damping offer a more realistic representation of structural dynamics than conventional linear models. Chatterjee and Chintha (2020) proposed an identification methodology employing

harmonic excitation to evaluate damping with third-order nonlinearity. Eberle (2025) presented a computationally economical and nonparametric method dedicated to the analysis of nonlinear damping. Furthermore, Han and Kinoshita (2012) introduced an indirect identification algorithm aimed at determining nonlinear damping vibrating systems with constant stiffness properties. The SLM was later extended to nonlinear systems by Lisitano and Bonisoli (2021), enabling the identification of nonlinear damping using frequency response functions (FRFs) obtained at different vibration amplitudes. In these developments, parametric excitation, such as time-varying stiffness, was not explicitly incorporated into the identification formulation. The results presented in these studies were obtained by assuming a constant mesh stiffness (Km), while the effect of stiffness variation was indirectly introduced through the dynamic response. However, the phenomenon of parametric excitation has attracted considerable attention in various fields of engineering due to its significant influence on the damping identification process (Sofroniou & Bishop, 2014). Parametric excitation arises from time-varying system parameters such as stiffness, mass, or damping (Belhaq *et al.*, 2013). In particular, time-varying stiffness may induce complex dynamic phenomena, including parametric resonance, instability regions, amplitude modulation, and nonlinear response amplification (Guo *et al.*, 2025). Such effects are frequently encountered in aeroelastic systems, civil engineering structures subjected to periodic loading, and rotating machinery (Chen *et al.*, 2024). Recent studies have demonstrated that stiffness variations significantly modify the dynamic characteristics and stability boundaries of mechanical systems (Li *et al.*, 2024). Therefore, neglecting time-varying stiffness in system modeling may lead to inaccurate parameter estimation, especially in damping identification problems. Consequently, the objective of this study is to develop a refined identification technique capable of estimating nonlinear damping in parametrically excited systems while explicitly accounting for the effects of time-varying stiffness. The originality of the proposed method is to extend the SLM for the estimation of nonlinear (SLMnl) damping, in multi-degree-of-freedom (MDOF) systems, while taking into consideration the effects of time-varying stiffness. The harmonic representation of the time-varying dynamic stiffness exploits multiple sidebands of the frequency response function simultaneously. Unlike conventional approaches based on the mean stiffness, the present technique reconstructs the equivalent stiffness matrix by combining the receptances computed at sideband frequencies. The periodic effects of stiffness are expressed through harmonic projections on a trigonometric basis, leading to a linear system $Aa = b$. This formulation makes full use of the information contained in multiple FRFs around the meshing frequency, enabling the simultaneous identification of linear and nonlinear damping coefficients as well as variable stiffness parameters with enhanced accuracy. The developed SLMnl, named the stabilized layers method for nonlinear damping with varying stiffness (SLMnl,kv), explicitly models time-varying stiffness and enables accurate identification of nonlinear damping in MDOF systems. The location of nonlinearity is detected by using nonlinearity location methods, and the time-varying stiffness model is presented by a periodic square wave function. A description of the SLMnl damping estimation with constant stiffness is given in Section 2. The limits of the SLMnl technique in the case of varying stiffness are presented in Section 3. The new SLMnl,kv is described in Section 4. In Section 5, SLMnl,kv is implemented for the identification of nonlinear damping and time-varying stiffness coefficients in spur gear pair systems.

2. Review of the SLMnl damping

The SLMnl presented by Lisitano and Bonisoli (2021) is an estimation technique for nonlinear damping with constant stiffness. A nonlinear damping that depends on the displacement amplitude A was expressed as

$$C(A) = C + C_{eq}(A) g g^T, \tag{2.1}$$

$$C_{eq} = c_{nl,0} g g^T + \ldots + c_{nl,m} g g^T, \tag{2.2}$$

where g is a vector indicating the location of nonlinear damping and A is the excitation amplitude. In the SLMnl, C is the non-proportional viscous damping. The nonlinear viscous damping $C_{eq}(A)$ was defined by

$$C_{eq}(A) = \sum_{m=0}^{M} v_m c_{nl,m} A^m. \tag{2.3}$$

Replacing the nonlinear viscous damping presented in Eq. (2.1) with Eq. (2.2), and rewriting it in the vector form, yields:

$$C(A) = C + C_{eq}(A) g g^T = \begin{bmatrix} C + c_{nl,0} g g^T \\ c_{nl,1} g g^T \\ \dots \\ c_{nl,m} g g^T \end{bmatrix}. \tag{2.4}$$

The proposed approach aims to estimate both the linear and nonlinear coefficients $c_{nl,0}, c_{nl,1}, ..., c_{nl,m}$ of the damping model C at $M+1$ amplitudes, where M represents the degree of nonlinearity. The equation of motion of the n-DOF system with nonlinear damping in the frequency domain subjected to an external excitation force $f(w)$ as a function of displacement $x(w)$ was presented as follows:

$$\left(K - w^2 M\right) x(w) + iw \left(C + C_{eq}(A) g g^T\right) x(w) = f(w), \tag{2.5}$$

where M, C, and $K \in R^{n,n}$ are the mass, viscous damping, and constant stiffness matrix of the system, respectively. The receptance frequency response matrix $H^R(w)$ was derived to identify the linear and nonlinear damping coefficients by using the following equation:

$$\left[wH^R(w)\right] \left[C + C_{eq}(A) g g^T\right] = G(A, w), \tag{2.6}$$

where $G(w)$ was determined from the equivalent linear damped $H^C(w)$ as follows:

$$G(A, w) = -H_I^C(A, w) \left[H_R^C(A, w)\right]^{-1}, \tag{2.7}$$

the equivalent linear damped H^C is presented by

$$H^C(w) = K - w^2 M + iw \left(C + C_{eq}(A) g g^T\right), \tag{2.8}$$

and $H_R^C(A, w)$ is the real part, and $H_I^C(A, w)$ is the imaginary part of the receptance $H^C \in C^{n,n}$. The dynamic stiffness matrix undamped H^R(w) was presented by the following equation:

$$\left[H^R(w)\right]^{-1} = K - w^2 M. \tag{2.9}$$

Equation (2.6) can be presented at $M + 1$ amplitudes by

$$\left[wH^R(w) wH^R(w) v^1 A \ \dots \ wH^R(w) v^M A^M\right] \left[C + C_{eq}(A) g g^T\right] = G(A, w). \tag{2.10}$$

In order to solve Eq. (2.10), the layers method was applied. The damping matrix is presented for relative and absolute dampers. The relative layer presents the connection between two DOFs, and the absolute layer represents the connection between the DOF and the external frame. Therefore, the linear damping matrix can be presented as the following sum of NL layers:

$$\mathbf{C} = \sum_{1}^{NL} \mathbf{C}_j = \sum_{p=1}^{NA} c_p \mathbf{P}_p^A + \sum_{p=1}^{NR} c_q \mathbf{P}_q^R; \quad \mathbf{C} = \left[P_1^A \dots P_{NA}^A P_1^R \dots P_{NR}^R\right] \begin{bmatrix} C_1 I \\ \dots \\ C_{NA} I \\ C_{NA+1} I \\ \dots \\ C_{NA+NR} I \end{bmatrix}, \tag{2.11}$$

where P_p^A and P_q^R are the absolute and relative patterns. M layers are added to represent the nonlinear damping coefficients $c_{nl,m}$. Therefore, Eq. (2.10) can be presented in the form:

$$\begin{bmatrix} V(A1) \\ V(A2) \\ \dots \\ V(AM+1) \end{bmatrix} \begin{bmatrix} P & & \\ & P_{nl} & \\ & & \dots \\ & & P_{nl} \end{bmatrix} \begin{bmatrix} c_1 I \dots c_{NA+NR} I \\ c_{nl,1} I \\ \\ c_{nl,M} I \end{bmatrix} = \begin{bmatrix} G(A1) \\ G(A2) \\ \dots \\ G(AM+1) \end{bmatrix}. \tag{2.12}$$

The first line of the matrix presents the viscous damping, and the M lines present the nonlinear damping coefficients. Finally, Eq. (2.12) was presented in the form $Aa = b$. Using the linear least square method, the unknown damping coefficients of the vector $a = [c_1 \dots c_{NA+NR} c_{nl,1} \dots c_{nl,M}]^T$ can be obtained. As presented in Eq. (2.12), stiffness was assumed to be constant, and the effect of time-varying stiffness was not explicitly incorporated into the damping identification. The SLMnl provides valuable contributions to damping identification, but it assumes a constant system, and therefore, neglects the influence of stiffness variation on the damping identification technique. Therefore, in the proposed technique presented in this study, all equations should be reformulated to identify nonlinear damping with time-varying stiffness. The extended algorithm is presented in Section 3.

3. Nonlinear-damped systems with time-varying stiffness

The equation of motion of n DOFs with nonlinear damping and time-varying stiffness can be written as follows:

$$M\ddot{x}(t) + C(A)\dot{x}(t) + (K + K(t))\, x(t) = f(t). \tag{3.1}$$

The damping matrix is presented by Eq. (2.1). The time-varying stiffness $K(t)$ presented in Fig. 1 is given by the following equation (Yousfi *et al.*, 2018):

$$K(t) = K_0 + \sum_{h=1}^{Nh} (K_h^c \cos(hw_m t) + K_h^s \sin(hw_m t)), \tag{3.2}$$

where K_h^c and K_h^s are the harmonic coefficients of the time-varying stiffness. Nh is the number of harmonic sidebands, and w_m is the mesh frequency. The oscillations observed in Fig. 1 result from the periodic representation of the time-varying mesh stiffness in the form of a Fourier series representation. This modulating variation creates additional components in the system's dynamic response, called sidebands, located around the excitation frequency ω. The number of

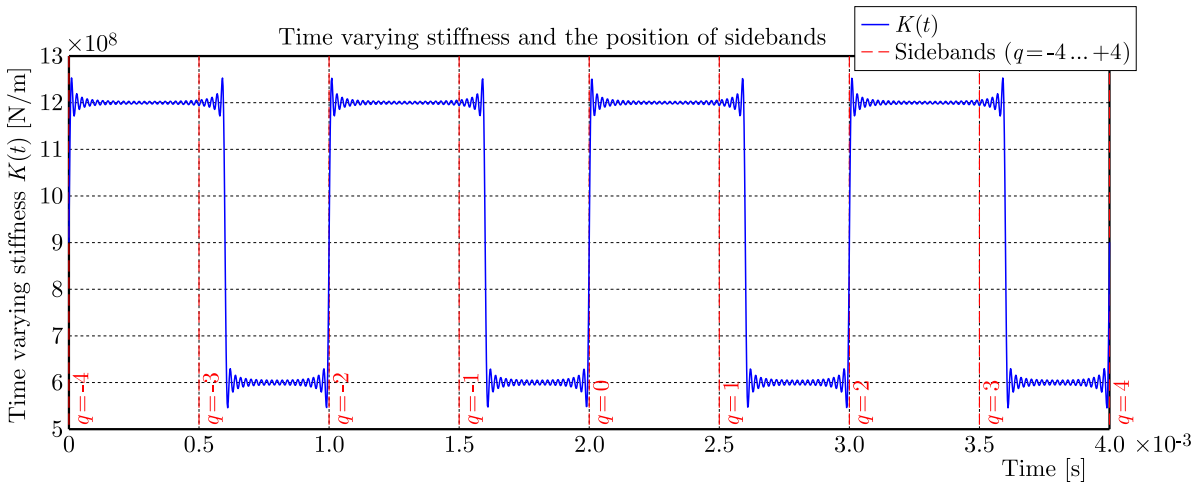

Fig. 1. Time varying stiffness.

sidebands is equal to $2Nh+1$. The sidebands are shown in Fig. 1 for $Nh=4$. These harmonics introduce local oscillatory fluctuations, especially near the transitions between single and double tooth contact regions. When such systems exhibit a nonlinear damping and time-varying stiffness, the dynamic behavior becomes even more complex, and the traditional SLMnl can affect the damping identification. The SLMnl is applied in a numerical example with varying stiffness in Section 3.1 to present its limits in identifying the nonlinear damping.

3.1. Limits of SLMnl damping identification in the case of time-varying stiffness

The SLMnl is applied to evaluate its limitations in the case of time-varying stiffness presented in Section 2. As an example, we consider a system with time-varying stiffness $K(t)$, the mass matrix M, and a viscous damping matrix C presented by

$$M=\begin{bmatrix}2&&\\&5&\\&&3\end{bmatrix},\qquad K=10^4\begin{bmatrix}5&3&0\\3&5&2\\0&2&1\end{bmatrix},\qquad C=10^5\begin{bmatrix}7&3&0\\3&8&2\\0&2&5\end{bmatrix},$$
$$f_{c,nl}=g(c_0+c_2x^2)\dot{x},\qquad c_0=140,\qquad c_2=1.35e5, \tag{3.3}$$

where $f_{c,nl}$ is the nonlinear damping force, and is applied on the first DOF, so that $g=(10\ 0)$. We added a time-varying stiffness, which can be modeled by a periodic square wave function presented in Eq. (3.2). In the method presented by Lisitano and Bonisoli (2021), the stiffness should be constant. Therefore, the mean value of $K(t)$ is considered. The first step of the SLMnl is to find the receptance function Hc, which is presented in Fig. 2. As it is presented, the system responses do not exhibit any signs of nonlinear behavior. As the excitation amplitude increases, the FRF curves remain almost superimposed, indicating that the response does not vary significantly with amplitude. This behavior suggests that the nonlinear damping effect is not properly identified, either. Consequently, the SLMnl approach fails to capture nonlinear damping when applied to systems with variable stiffness and using the mean value of stiffness. Figure 3 and Fig. 4 present damping coefficients identified at low and high frequencies. At low

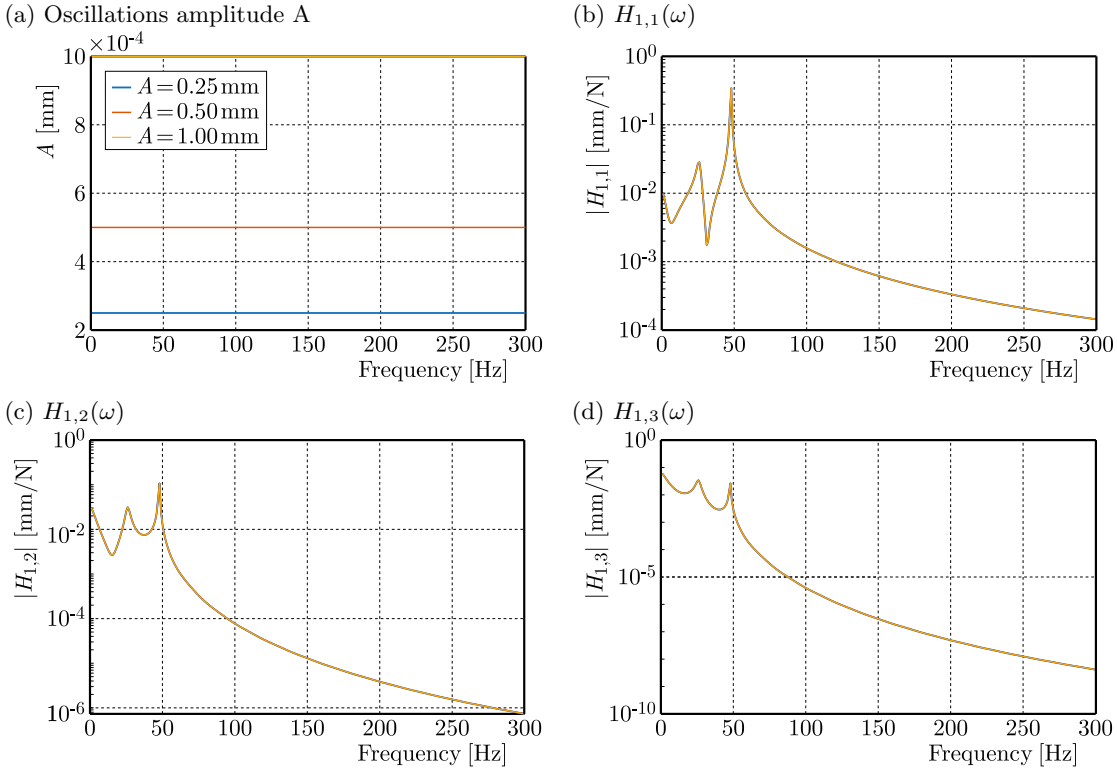

Fig. 2. Frequency response functions (FRFs) obtained with SLMnl.

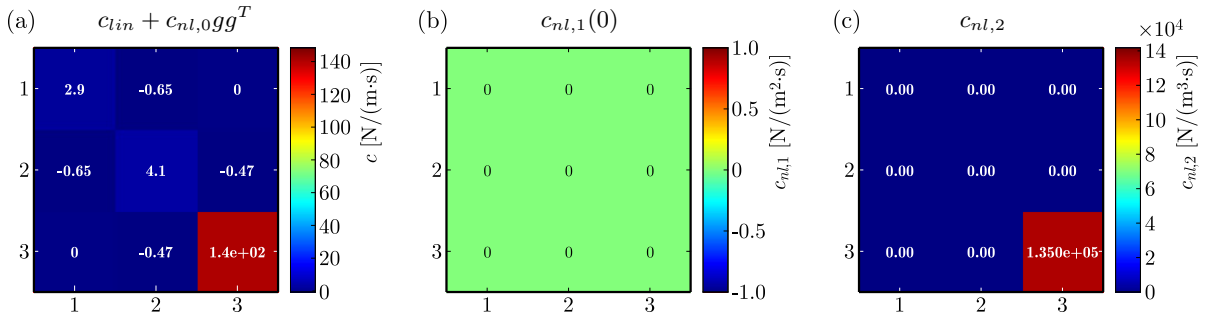

Fig. 3. Damping coefficients at low frequency computed with SLMnl.

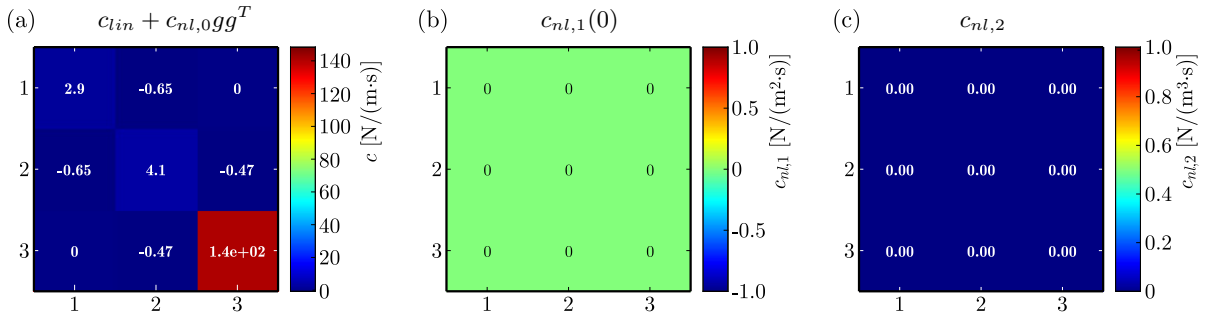

Fig. 4. Damping coefficients at high frequency computed with SLMnl.

frequency, a good correspondence is obtained with the real nonlinear coefficients $c_0 = 140$, $c_2 = 1.35e5$. However, the nonlinear coefficient c_2 identified by the SLMnl at high frequency is zero, different from the real value $c_2 = 1.35e5$. Therefore, this result suggests that, under low-frequency excitation, the system response remains sufficiently dominated by the modeled nonlinear damping effects, and the underlying assumptions of the SLMnl formulation remain valid. In contrast, at high frequency, the nonlinear damping coefficient c_2 identified by the SLMnl collapses to zero, which is a significant deviation from its true value. This behavior highlights a clear limitation of the SLMnl approach when applied to high-frequency dynamics. At elevated frequencies, the system response becomes increasingly influenced by inertial effects and higher-order dynamic interactions, which can mask the contribution of nonlinear damping. As a result, the SLMnl fails to properly isolate and estimate the nonlinear damping component. Overall, these results demonstrate that the SLMnl is highly sensitive to the selected frequency range. While it provides reliable damping identification at low frequencies, its performance degrades significantly at high frequencies due to the combined effects of unmodeled stiffness variations and reduced observability of nonlinear damping. Consequently, the SLMnl formulation presented by Lisitano and Bonisoli (2021) assumes a constant stiffness, and its applicability is limited for systems with time-varying stiffness, particularly at higher frequencies. For accurate damping estimation over a wide frequency range, it is necessary to extend the SLMnl formulation presented by Lisitano and Bonisoli (2021) to explicitly incorporate time-varying mesh stiffness. Therefore, the novelty of the present work lies in reformulating the SLMnl to add a time-varying stiffness effect. The proposed method is presented in Section 4.

4. Nonlinear damping identification in the case of time-varying stiffness

4.1. Stabilized layers method for nonlinear damping with varying stiffness (SLMnl,kv)

The equation of motion of the n-DOF system with nonlinear damping and time-varying stiffness can be expressed in the frequency domain as follows:

$$M\ddot{x}(w) + iw(C + C_{eq}(A) g g^T)x(w) + (K + K(w_m))\, x(w) = f(w), \tag{4.1}$$

where $f_{c,nl} = iwC_{eq}(A)gg^T$ is the nonlinear damping force, $x(w)$ is the displacement in the frequency domain, and $f(w)$ is the excitation force in the frequency domain. C_{eq} is the nonlinear damping matrix given by Eq. (2.4). The time-varying stiffness $K(t)$ is given by Eq. (3.2). The idea of the proposed SLMnl,kv is to identify the harmonic coefficients K_h^c and K_h^s together with the linear and nonlinear coefficients. Therefore, two vectors must be identified. One is a vector which contains the harmonic coefficients of the time-varying stiffness defined by

$$\kappa = \left[\kappa_{c,1}, \kappa_{s,1}, ..., \kappa_{c,Nh}, \kappa_{s,Nh}\right]^T, \tag{4.2}$$

and the other is a vector which contains the linear and nonlinear coefficients of the damping, as follows:

$$u_{lin+nl} = \left[c_1, ..., c_{NA+NR}, c_{nl,1}, ..., c_{nl,M}\right]^T. \tag{4.3}$$

The periodic variation of the stiffness $K(t)$ acts as a parametric excitation that modulates the vibration response of the system, resulting in the appearance of frequency sidebands (at $\pm w_m$, $\pm 2w_m$, ...) around the central excitation frequency w_m. Therefore, the selection of a frequency range around w_m can overcome the limits of the current SLMnl. The frequency range was selected around each sideband. The frequency range is presented by $w_{q,i} = w_i + qw_m$, $q \in \{-Nh, ..., Nh\}$, $i \in \{1, ..., K\}$. The dynamic stiffness matrix of the undamped system around each sideband $H^R(w_q)$ can be presented as follows:

$$\left[H^R(w_q)\right]^{-1} = K - w_q^2 M, \tag{4.4}$$

by multiplying Eq. (4.1) by $H^R(w_q)$, we obtain:

$$\begin{aligned} &x(w_q) + H^R(w_q)\left(iw_q\left(C + C_{eq}(A)gg^T\right)\right)x(w_q) \\ &\quad + \left(\sum_{h=1}^{Nh} H^R(w_q)\left(K_h^c \cos(hw_m t) + K_h^s \sin(hw_m t)\right)\right)x(w_q) = H^R(w_q)f(w_q). \end{aligned} \tag{4.5}$$

Here, the product $H^R(w_q)\left(iw_q C(A)\right)$ naturally appears to indicate that it originates from the damping term, and the terms $\sum_{h=1}^{Nh} H^R(w_q)\left(K_h^c \cos(hw_m t) + K_h^s \sin(hw_m t)\right)$ arise from the modulation of time-varying stiffness $K(t)$.

Therefore, the vector of displacement can be presented as follows:

$$\begin{aligned} x(w_q) = &\Bigg[1 + H^R(w_q)\left(iw_q C + C_{eq}(A)gg^T\right) \\ &+ \left(\sum_{h=1}^{Nh} H^R(w_q)\left(K_h^c \cos(hw_m t) + K_h^s \sin(hw_m t)\right)\right)\Bigg]^{-1} H^R(w_q)f(w_q). \end{aligned} \tag{4.6}$$

The transformation matrix $G(A, w_q)$ can be presented by

$$\begin{aligned} G(A, w_q) = &w_q H^R(w_q)\left(C + C_{eq}(A)gg^T\right) \\ &+ \left(\sum_{h=1}^{Nh} H^R(w_q)\left(K_h^c \cos(hw_m t) + K_h^s \sin(hw_m t)\right)\right). \end{aligned} \tag{4.7}$$

At this stage, the stiffness modulation generates additional sideband coupling terms in the system equations. Specifically, the dissipative contribution $V_q(w_q, A) \in \mathbb{R}^{n,n}$, which is a complex block matrix associated with the q-th sideband, is defined, and the modulated contribution is

presented by the vector $\nu_q \in \mathbb{R}^{n,n}$ due to the time-varying stiffness associated with the q-th sideband. These terms modify the block matrix structure. Such modulation-induced terms do not appear in the method proposed by Lisitano and Bonisoli (2021), since their model assumes constant stiffness and therefore does not generate time-periodic coefficients.

Therefore, for each sideband, we can write:

$$G(A, w_q) = V_q(w_q, A)\left(C + C_{eq}(A) g g^T\right) + \nu_q(w_q, A)\left(\sum_{h=1}^{Nh}\left(K_h^c \cos(h w_m t) + K_h^s \sin(h w_m t)\right)\right). \tag{4.8}$$

To transform Eq. (4.7) into the matrix form, we used the vector of harmonic coefficients presented by Eq. (4.2). Then, we introduced two vectors for cosine and sine combinations:

$$\begin{aligned} P_c^{(h)} &= \sum_{h=1}^{Nh} \cos(h w_m t)\nu_q(w_q, A), \\ P_s^{(h)} &= \sum_{h=1}^{Nh} \sin(h w_m t)\nu_q(w_q, A). \end{aligned} \tag{4.9}$$

The vectors of cosine and sine combinations are arranged in the matrix $A_\kappa \in \mathbb{C}^{n^2 \times N_k}$ with $N_k = 2Nh$ defined by

$$A_\kappa = \left[P_c^1, P_s^1, ..., P_c^{Nh}, P_s^{Nh}\right]. \tag{4.10}$$

By substituting the definition of time-varying stiffness with Eq. (3.2) and Eq. (4.9), and replacing the definition of the nonlinear viscous damping coefficients with Eq. (2.4), a matrix form of Eq. (4.7) is written in the frequency range $w_{q,i} = w_i + q w_m$, $q \in \{-Nh, ..., Nh\}$, $i \in \{1, ..., K\}$:

$$\begin{bmatrix} w_q H_R(w_{q,1}) \\ w_q H_R(w_{q,2}) v_1 A^1 \\ ... \\ w_q H_R(w_{q,K}) v_M A^M \end{bmatrix} \begin{bmatrix} C + c_{nl,0} g g^T \\ c_{nl,1} g g^T \\ ... \\ c_{nl,m} g g^T \end{bmatrix} + \begin{bmatrix} P_c^1 \\ P_s^1 \\ ... \\ P_c^{Nh} \\ P_s^{Nh} \end{bmatrix} \begin{bmatrix} \kappa_{c,1} \\ \kappa_{s,1} \\ \\ \kappa_{c,Nh} \\ \kappa_{s,Nh} \end{bmatrix} = \begin{bmatrix} G(A, w_{q,1}) \\ G(A, w_{q,2}) \\ ... \\ G(A, w_{q,K}) \end{bmatrix}. \tag{4.11}$$

Let

$$V(A) = \begin{bmatrix} w_q H_R(w_{q,1}) \\ w_q H_R(w_{q,2}) v_1 A^1 \\ ... \\ w_q H_R(w_{q,K}) v_M A^M \end{bmatrix} \in \mathbb{R}^{nK, n(M+1)}, \quad G(A) = \begin{bmatrix} G(A, w_{q,1}) \\ G(A, w_{q,2}) \\ ... \\ G(A, w_{q,K}) \end{bmatrix} \in \mathbb{R}^{nK, n}.$$

The layers method presented in Section 2 by Eq. (2.11) was applied for $M + 1$ different values of the amplitude A. The following equation can be obtained:

$$\overline{VP} \begin{bmatrix} c_1 I ... c_{NA+NR} I \\ c_{nl,1} I \\ \\ c_{nl,M} I \end{bmatrix} + A_\kappa \begin{bmatrix} \kappa_{c,1} \\ \kappa_{s,1} \\ \\ \kappa_{c,Nh} \\ \kappa_{s,Nh} \end{bmatrix} = \overline{G}, \tag{4.12}$$

where

$$\overline{V(A)} = \begin{bmatrix} V_q(A1) \\ V_q(A2) \\ ... \\ V_q(AM+1) \end{bmatrix} \mathbb{R}^{nK(M+1), n(M+1)}, \qquad \overline{G}(A) = \begin{bmatrix} G(A1) \\ G(A2) \\ ... \\ G(AM+1) \end{bmatrix} \in \mathbb{R}^{nK(M+1), n},$$

$$\overline{P} = \begin{bmatrix} P & & & \\ & P_{nl} & & \\ & & .. & \\ & & & P_{nl} \end{bmatrix} \in \mathbb{R}^{n^2 K(M1), NA+NR+M}.$$

In order to identify the harmonic coefficients $\kappa = [\kappa_{c,1}, \kappa_{s,1}, ..., \kappa_{c,Nh}, \kappa_{s,Nh}]^T$ and the linear and nonlinear damping coefficients $u_{lin+nl} = [c_1, ..., c_{NA+NR} c_{nl,1}, ..., c_{nl,M}]^T$, the matrices $Zi \in \mathbb{R}^{n(NA+NR+M),(NA+NR+M)}$ and $Yi \in \mathbb{R}^{n,1}$ are introduced to isolate the correct coefficients in the vector u_{lin+nl}. Zi is associated with the coefficients in $\overline{V}$, and Yi is associated with those in $\overline{G}$. They mostly contain 0 and 1, used to pick out the relevant terms for each equation:

$$\begin{aligned} &Zi = 0 \quad \text{and} \quad (Zi)_{(y-1)_{n,y}} = 1 \quad \text{with} \quad y = 1, ..., NA + NR + M, \\ &Yi = 0 \quad \text{and} \quad (Yi)_{i,1} = 1. \end{aligned} \tag{4.13}$$

Equation (4.12) can be presented as follows:

$$\begin{bmatrix} \overline{VP}Z1 \\ \overline{VP}Z2 \\ ... \\ \overline{VP}Zn \end{bmatrix} u_{lin+nl} + A_\kappa \kappa = \overline{G}. \tag{4.14}$$

A summation is carried out over all Nh sidebands:

$$\sum_{1}^{Nh} \begin{bmatrix} \overline{VP}Z1 \\ \overline{VP}Z2 \\ ... \\ \overline{VP}Zn \end{bmatrix} u_{lin+nl} + \sum_{1}^{Nh} A_\kappa \kappa = \overline{Q}. \tag{4.15}$$

Finally, we introduced the matrix form $Aa = b$, which can be solved using the linear least squares method:

$$\sum_{1}^{Nh} \begin{bmatrix} A_{lin+nl}(A, w_q) & A_\kappa(A, w_q) \end{bmatrix} \begin{bmatrix} u_{lin+nl} \\ \kappa \end{bmatrix} = \text{vec}\,(Q(A, w_q)), \tag{4.16}$$

where

$$A_{lin+nl}(A, w_q) = \begin{bmatrix} \overline{VP}Z1 \\ \overline{VP}Z2 \\ ... \\ \overline{VP}Zn \end{bmatrix}.$$

We can conclude that, in the SLMnl,kv, the effect of time-varying stiffness is introduced in the identification formulation compared with the SLMnl, which neglected the time-varying stiffness effect. The last step of the proposed technique is to verify its reliability using a global stability matrix for different amplitudes and spectral lines K:

$$S = \bigcap_{h=1}^{NA+NR+M} S_h, S_h(k, r) = 1 \quad \text{if} \quad \frac{c_{hkr} - c_{hk+jr+i}}{c_{hkr}} \leq \varepsilon \forall (i, j) = \pm 1. \tag{4.17}$$

4.2. Numerical example

In order to prove the suitability of the new SLMnl,kv for damping identification in the case of time-varying stiffness, a numerical example presented in Section 3 is used. The steps of the SLMnl,kv are applied. Figure 5 presents the damping matrices identified by the SLMnl,kv at high frequency. A good correspondence is obtained with the damping matrices of Eq. (3.3). We can conclude that the SLMnl,kv approach overcomes the limitations of the SLMnl through its new formulation, which explicitly considers the effect of stiffness variation by defining spectral frequency w_q.

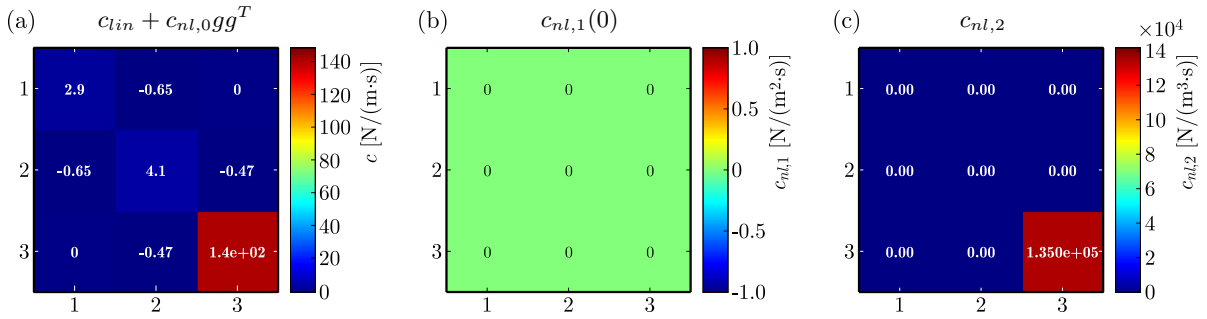

Fig. 5. Damping coefficients at high frequency computed with SLMnl,kv.

5. Identification of nonlinear damping in spur gear pair system

The SLMnl,kv, proposed in Section 4, is applied in a spur gear pair system. The numerical response employed in this work is obtained using the dynamic model described in the dynamic analysis of spur gear systems presented by Wei *et al.* (2021), which has been experimentally validated on a dedicated test bench. In that study, the simulated vibration responses were compared with measured data, showing a good agreement in both time and frequency domains. The values of the mass, stiffness, and gear variables are obtained from this reference model, and the vibration signal is derived through the numerical integration of the model equations. In Section 5.1 the linear structural damping and nonlinear damping due to the interaction between the pinion and gear are identified using the proposed SLMnl,kv.

5.1. Model of spur gear pair system

The dynamic model of the spur gear pair system is presented in Fig. 6. The system is composed of a gear, pinion, load, and motor. The contact between the pinion and the motor is represented by torsional stiffness k_{c1} and torsional damping c_{c1}, while k_{c2} and c_{c2} represent the contact between the gear and the load. k_{x1}, k_{y1}, c_{x1}, and c_{y1} are the equivalent support stiffness and the equivalent support damping in the two directions, x and y, of the pinion. k_{x2}, k_{y2}, c_{x2}, and c_{y2} are the equivalent support stiffness and the equivalent support damping in the two directions, x and y, of the gear. The dampers c_{x1}, c_{y1}, c_{x2}, and c_{y2}, which are not plotted in

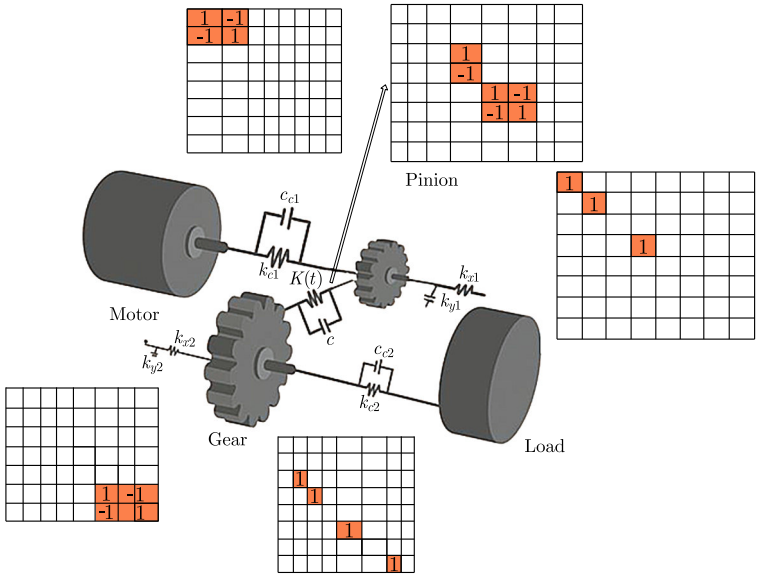

Fig. 6. Absolute and relative layers representation.

Fig. 6, will be given in the equation of motion. The mesh damping model utilized in this study is quadratic nonlinear with the nonlinear damping force, as follows:

$$f_{cnl} = \left(c_{nl,0} + c_{nl,2}x^2\right)\dot{x}, \tag{5.1}$$

where

$$c_{nl,0} = 240 \qquad \text{and} \qquad c_{nl,2} = 2.4e8.$$

θm, θ_1, θ_1, θ_L are the angular displacements of the motor, the pinion, the gear, and the load. x_1, y_1, x_2, y_2 are the displacements of the pinion and the gear in the x-, y-directions. Therefore, the system presents 8 DOFs. The equation of motion of the spur gear pair system is given by

$$M\ddot{x}(t) + (C + C_b)\,\dot{x}(t) + (Kb + K(t))\,x(t) = f(t), \tag{5.2}$$

where $x(t)$ represents the displacement vector expressed as

$$x(t) = [x_1, y_1, \theta m, \theta_1, \theta_1, \theta_L, x_2, y_2], \tag{5.3}$$

$f(t)$ is the excitation force, M is the mass matrix, and C_b is structural damping. The contact between the gear and the pinion is modeled by a time-varying stiffness and structural stiffness $K = K(t) + Kb$, where $K(t)$ is the time-varying stiffness presented in Section 2 by Eq. (3.2) as follows:

$$M = \begin{bmatrix} m_1 & & & & & & & \\ & m_1 & & & & & & \\ & & I_m & & & & & \\ & & & I_1 & & & & \\ & & & & m_2 & & & \\ & & & & & m_2 & & \\ & & & & & & I_L & \\ & & & & & & & I_2 \end{bmatrix}, \tag{5.4}$$

$$K_b = \begin{bmatrix} k_{x1} & & & & & & & \\ & k_{y1} & & & & & & \\ & & k_{c1} & -k_{c1} & & & & \\ & & -k_{c1} & k_{c1} & & & & \\ & & & & k_{x2} & & & \\ & & & & & k_{y2} & & \\ & & & & & & k_{c2} & -k_{c2} \\ & & & & & & -k_{c2} & k_{c2} \end{bmatrix}, \tag{5.5}$$

$$C_b = \begin{bmatrix} c_{x1} & & & & & & & \\ & c_{y1} & & & & & & \\ & & c_{c1} & -c_{c1} & & & & \\ & & -c_{c1} & c_{c1} & & & & \\ & & & & c_{x2} & & & \\ & & & & & c_{y2} & & \\ & & & & & & c_{c2} & -c_{c2} \\ & & & & & & -c_{c2} & c_{c2} \end{bmatrix}.$$

5.2. Nonlinear damping identification

The nonlinear damper is located at the contact between the pinion and the gear. Therefore, $g = [0\ 0\ 0\ 10\ 0\ 0\ 1]$. The degree of nonlinearity $M = 2$. The SLMnl,kv is applied for 3 amplitudes $A = [0.25\ 0.5\ 1]$. Two absolute layers are defined to present the contact between the pinion support, and the contact gear support. Three relative layers are defined to show the pinion-motor, pinion-gear and gear-load contacts. Two layers $P_{nl} = gg^T$ are defined to identify the nonlinear coefficients. All layers are presented in Fig. 7.

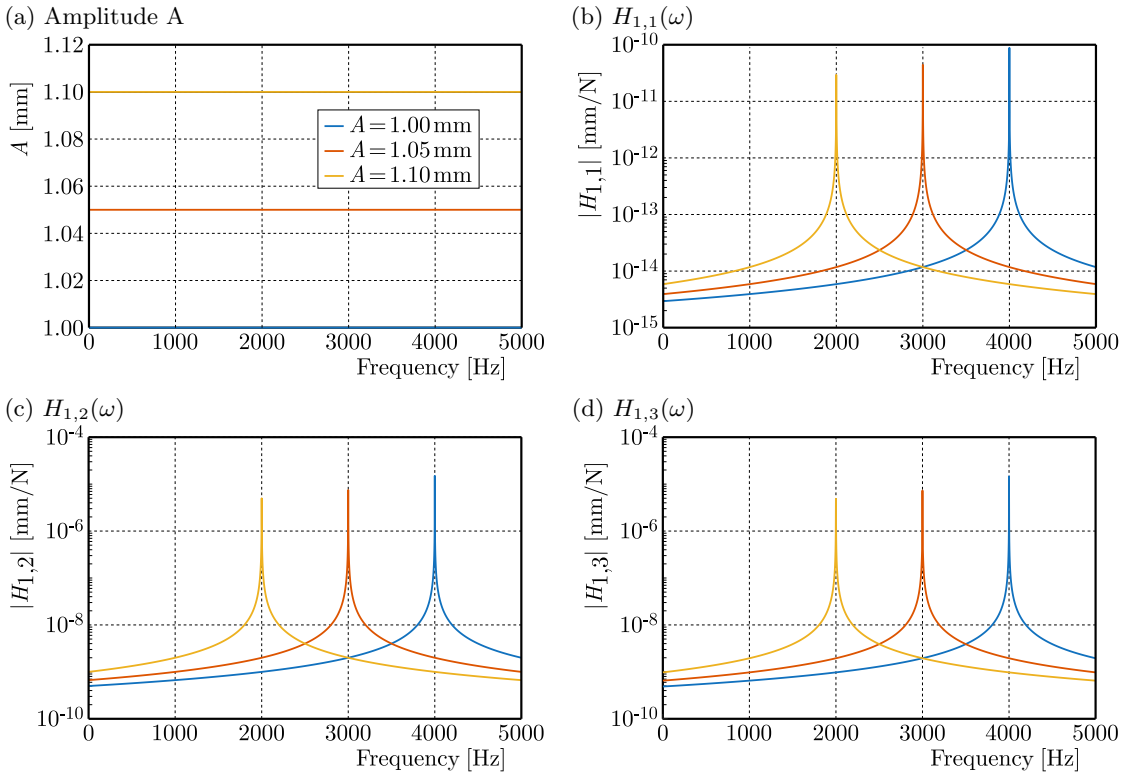

Fig. 7. Frequency response functions (FRFs) obtained with SLMnl,kv.

We defined the vector composed by linear and nonlinear damping coefficient:

$$u_{lin+nl} = \left[\frac{c_{x1} + c_{y1}}{2}, \frac{c_{x2} + c_{y2}}{2}, c_{c1}, c_{nl,0}, c_{c2}, c_{nl,1}, c_{nl,2}\right]. \tag{5.6}$$

The frequency range is presented by $w_{q,i} = w_i + qw_m$, $q \in \{-Nh, ..., Nh\}$, $i \in \{1, ..., K\}$, where $w_m = \frac{2\pi}{T_1}$, T_1 represents the mesh period of the gear system calculated by $T_1 = \frac{60}{NZ_1}$, where N is the input rotational speed and z_1 is the tooth number of the pinion. The first step of the SLMnl,kv is to find the receptance function Hc, which is presented in Fig. 7. We can conclude that the effects of nonlinearity are visible. As the amplitude A increases, both the second and third peaks decrease in amplitude and move toward lower frequencies, while the first peak remains essentially unchanged. The FRFs exhibit a pronounced amplitude dependency, characterized by a progressive shift of resonance frequencies toward lower values as the excitation amplitude increases. This behavior indicates a dominant softening nonlinearity induced by the gear mesh stiffness variation. Moreover, the limited growth of resonance peaks at higher amplitudes highlights the presence of nonlinear damping mechanisms. Figure 8 presents the identified linear damping matrices, the damping values obtained using the SLMnl,kv correspond closely to the reference values $c_{nl,0} = 240$, confirming the accuracy of the proposed identification strategy for linear dissipation. Figure 9a presents the nonlinear damping coefficient $c_{nl,1}$, which corresponds to the real value $c_{nl,1} = 0$, indicating that the method is able to capture the first-order

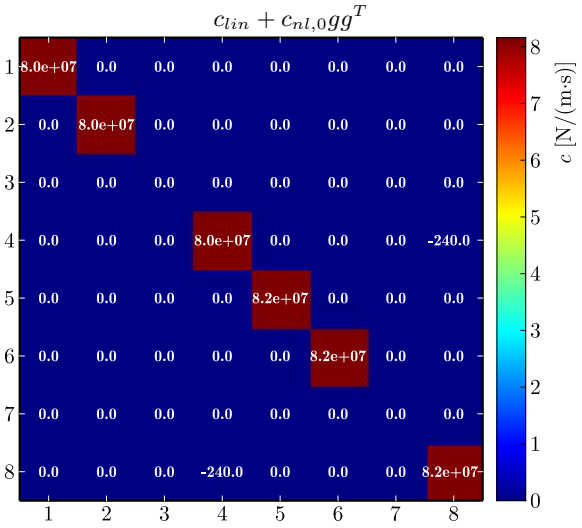

Fig. 8. Linear damping coefficients computed with SLMnl,kv.

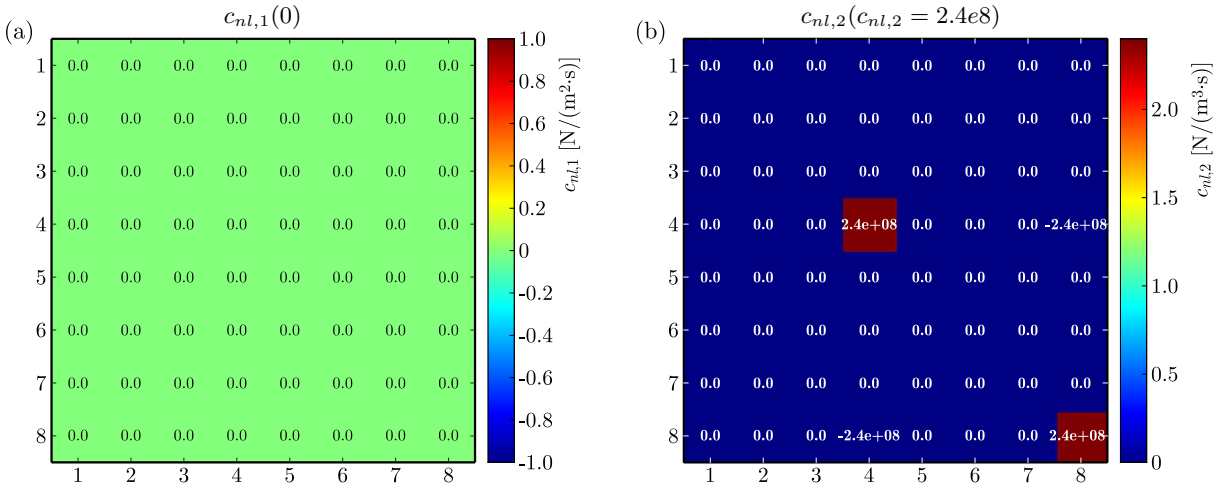

Fig. 9. (a) Nonlinear damping coefficient $c_{nl,1}$ computed with SLMnl,kv; (b) nonlinear damping coefficient $c_{nl,2}$ computed with SLMnl,kv.

nonlinear dissipation mechanism associated with the gear mesh. Figure 9b presents the nonlinear damping coefficient $c_{nl,2}$, which corresponds to the real value $c_{nl,2} = 2.4e8$, demonstrating the capability of the method to identify higher-order nonlinear effects. From the obtained results, linear and nonlinear coefficients can be correctly estimated using the proposed new formulation of the SLMnl,kv technique. Therefore, the option that the damping identification is performed in each frequency range $w_{q,i} = w_i + qw_m$, $q \in \{-Nh, ..., Nh\}$, $i \in \{1, ..., K\}$ helps find the real linear and nonlinear damping coefficients. Furthermore, performing the damping identification separately within each frequency range significantly improves the robustness of the estimation, as it allows the method to account for amplitude-dependent stiffness variations and localized resonance phenomena. This frequency-dependent identification strategy enhances the physical consistency of the identified parameters and enables an accurate reconstruction of the system's dynamic behavior across different operating conditions.

6. Conclusion

A new technique is proposed of nonlinear damping estimation in a mechanical system with n DOFs in the case of time-varying stiffness. The time-varying stiffness is characterized by a pe-

riodic variation around the excitation frequency w_m, which leads to the appearance of Nh sidebands in the system's response. Each sideband is characterized by a spectral frequency around each frequency. If the effect of the time-varying stiffness is not considered during the damping identification process, as it is presented in the traditional methods, significant estimation errors may arise due to the modulation of the dynamic behavior of the system. Therefore, an appropriate consideration of time-varying stiffness effects leads to a better identification of the linear and nonlinear damping coefficients. The idea of this research is to account for the time-varying stiffness on sidebands. Then, the estimation process is applied in each sideband. The identified harmonic coefficients and linear and nonlinear damping coefficients are obtained by summation over all sidebands. Since the gear systems are characterized by a time-varying stiffness, the SLMnl,kv is applied to estimate nonlinear damping in the spur gear pair system. In conclusion, the proposed SLMnl,kv approach offers a promising solution for the estimation of nonlinear damping in dynamic systems. Future work can focus on further refining this method to test its applicability to identifying damping in the case of backlash, including experimental validation, where contact loss and re-engagement introduce strong nonlinearities and piecewise stiffness variations. Incorporating such effects into the identification framework would enable the assessment of the method's robustness under more complex dynamic conditions.

References

1. Al-hababi, T., Cao, M., Saleh, B., Alkayem, N.F., & Xu, H. (2020). A critical review of nonlinear damping identification in structural dynamics: Methods, applications, and challenges. *Sensors*, *20*(24), Article 7303. https://doi.org/10.3390/s20247303
2. Amabili, M., Alijani, F., & Delannoy, J. (2016). Damping for large-amplitude vibrations of plates and curved panels, part 2: Identification and comparisons. *International Journal of Non-Linear Mechanics*, *85*, 226–240. https://doi.org/10.1016/j.ijnonlinmec.2016.05.004
3. Balasubramanian, P., Ferrari, G., & Amabili, M. (2018). Identification of the viscoelastic response and nonlinear damping of a rubber plate in nonlinear vibration regime. *Mechanical Systems and Signal Processing*, *111*, 376–398. https://doi.org/10.1016/j.ymssp.2018.03.061
4. Belhaq, M., Kirrou, I., & Mokni, L. (2013). Periodic and quasiperiodic galloping of a wind-excited tower under external excitation. *Nonlinear Dynamics*, *74*(3), 849–867. https://doi.org/10.1007/s11071-013-1010-9
5. Bonisoli, E., Lisitano, D., & Vigliani, A. (2019). Damping identification and localisation via Layer Method: Experimental application to a vehicle chassis focused on shock absorbers effects. *Mechanical Systems and Signal Processing*, *116*, 194–216. https://doi.org/10.1016/j.ymssp.2018.06.013
6. Chatterjee, A., & Chintha, H.P. (2020). Identification and parameter estimation of cubic nonlinear damping using harmonic probing and Volterra series. *International Journal of Non-Linear Mechanics*, *125*, Article 103518. https://doi.org/10.1016/j.ijnonlinmec.2020.103518
7. Chen, R., Lv, J., Tian, J., Ai, Y., Zhang, F., & Yao, Y. (2024). Modeling and nonlinear dynamic characteristics analysis of fault bearing time-varying stiffness-flexible rotor coupling system. *Mathematics*, *12*(22), Article 3591. https://doi.org/10.3390/math12223591
8. Clough, R.W., & Penzien, J. (1993). *Dynamics of structures* (2nd ed.). McGraw-Hill.
9. Eberle, R. (2025). Estimating nonlinear damping for mechanical single-degree-of-freedom systems: A robust and effective approach. *Proceedings in Applied Mathematics and Mechanics*, *25*(1), Article e202400158. https://doi.org/10.1002/pamm.202400158
10. Guo, Z., Zhang, Y., Sheng, M., Liu, L., & Li, Y. (2025). Vibration characteristics of a beam with elastic time-varying stiffness boundaries. *Applied Sciences*, *15*(21), Article 11365. https://doi.org/10.3390/app152111365
11. Haghdoust, P., Lo Conte, A., Cinquemani, S., & Lecis, N. (2018). A numerical method to model non-linear damping behaviour of martensitic shape memory alloys. *Materials*, *11*(11), Article 2178. https://doi.org/10.3390/ma11112178

12. Han, S.L., & Kinoshita, T. (2012). Nonlinear damping identification in nonlinear dynamic system based on stochastic inverse approach. *Mathematical Problems in Engineering*, *2012*(1), 1–20, Article 574291. https://doi.org/10.1155/2012/574291

13. Li, C., Hao, J., Liu, H., Hua, C., & Yao, Z. (2024). Nonlinear parametric vibration and stability analysis of worm drive system with time-varying meshing stiffness and backlash. *Journal of Sound and Vibration*, *575*, Article 118264. https://doi.org/10.1016/j.jsv.2024.118264

14. Lisitano, D., & Bonisoli, E. (2021). Direct identification of nonlinear damping: application to a magnetic damped system. *Mechanical Systems and Signal Processing*, *146*, Article 107038. https://doi.org/10.1016/j.ymssp.2020.107038

15. Lisitano, D., Bonisoli, E., & Mottershead, J.E. (2018). Experimental direct spatial damping identification by the Stabilised Layers Method. *Journal of Sound and Vibration*, *437*, 325–339. https://doi.org/10.1016/j.jsv.2018.08.055

16. Liu, Q., Wang, Y., Sun, P., & Wang, D. (2022). Comparative analysis of viscous damping model and hysteretic damping model. *Applied Sciences*, *12*(23), Article 12107. https://doi.org/10.3390/app122312107

17. Paz, M. (1991). Structural dynamics: Theory and computation (3rd ed.). Van Nostrand Reinhold.

18. Qu, C., Tu, G., Gao, F., Sun, L., Pan, S., & Chen, D. (2024). Review of bridge structure damping model and identification method. *Sustainability*, *16*(21), Article 9410. https://doi.org/10.3390/su16219410

19. Sofroniou, A., & Bishop, S. (2014). Dynamics of a parametrically excited system with two forcing terms. *Mathematics*, *2*(3), 172–195. https://doi.org/10.3390/math2030172

20. Wei, S., Chu, F.-L., Ding, H., & Chen, L.-Q. (2021). Dynamic analysis of uncertain spur gear systems. *Mechanical Systems and Signal Processing*, *150*, Article 107280. https://doi.org/10.1016/j.ymssp.2020.107280

21. Yousfi, N., Zghal, B., Akrout, A., Walha, L., & Haddar, M. (2018). Damping models identification of a spur gear pair. *Mechanism and Machine Theory*, *122*, 371–388. https://doi.org/10.1016/j.mechmachtheory.2018.01.002

22. Zahid, F.B., Ong, Z.C., & Khoo, S.Y. (2020). A review of operational modal analysis techniques for in-service modal identification. *Journal of the Brazilian Society of Mechanical Sciences and Engineering*, *42*(8), Article 398. https://doi.org/10.1007/s40430-020-02470-8

Manuscript received December 27, 2025; accepted for publication March 25, 2026; published online May 21, 2026.